crystals

MDPI

Article

Layered Hybrid iron Fluorides

Teng Li and Philip Lightfoot *

School of Chemistry and EaStChem, University of St Andrews, St Andrews KY16 9ST, UK
* Correspondence: pl@st-andrews.ac.uk; Tel.: +44-1334-463841

Abstract: The first examples of layered hybrid iron fluorides are reported. In the reactions carried out, the chain compound (H_2*pipz*)$FeF_5 \cdot H_2O$ always occurs as the major phase, with the layered compounds, (H_2*pipz*)$_3Fe_4F_{18} \cdot 2H_2O$ and (H_2*pipz*)$_2Fe_3F_{13} \cdot H_2O$, being isolated from some reactions as major impurities. The latter two compounds feature two-dimensional sheets of corner- and edge-shared $FeIIIF_6$ octahedra, resulting in two distinct layer architectures. The compound (H_2*pipz*)$FeF_5 \cdot H_2O$, isolated as the major phase, crystallises with a one-dimensional structure exhibiting zig-zag $[FeF_5]_\infty$ chains. This work opens up the potential for a much wider family of layered hybrid transition-metal fluorides.

Keywords: iron fluorides; hybrid compounds; crystal structure

1. Introduction

The exploration of hybrid metal halide chemistry has flourished in recent years, due to the potential of such compounds as functional materials, most famously the lead halide perovskites, for example in solar cell applications. The lead halides display a remarkably diverse structural chemistry, incorporating both 3D and layered perovskite-like structures, but also a wider array of lower-dimensional structure types based on layers, chains or isolated polyhedral units [1–3]. Metals other than lead have also been incorporated into hybrid systems, with a similarly large and expanding diversity of compositions and structures. Thus, there are many examples of 3*d*, and even 4*d*, cations being incorporated into layered hybrid perovskites, for example [4–7]. Astonishingly, however, work in all these systems has focussed almost exclusively on the heavier halides, Cl, Br or I. Although there are many examples of compounds containing isolated MF_6 octahedral units in hybrid fluoride chemistry [8,9], there are only a handful of examples of two-dimensional or higher connectivity of polyhedral units (typically MF_6 octahedra) in such systems. An earlier review found only three examples of hybrid transition-metal fluorides with two-dimensional connectivity of linked MF_6 octahedra [9]. Specifically these compounds were $[H_2en]ScF_4$ (*en* = 1,2-diaminoethane) [10], $[H_2pipz]_2Mn_4F_{16}$ (*pipz* = piperazine) [11] and $[Hgua]_2Fe_5F_{17}$ (*gua* = guanidine); the latter compound appears not to have been published. There are apparently very few more recent examples of layered transition metal fluorides based on linked MF_6 octahedra; indeed we can only find two further examples, *viz.* $(NH_4)_2[Hea]V_3F_{12}$ (*ea* = ethylammonium) [12], which has a kagome-like layer and $[H_2en]MnF_4$, which has a layered perovskite-like structure [13]. Figure 1 illustrates the inorganic layers in these four previously reported examples. We note further that hybrid fluorides based on linked polyhedra other than MF_6 octahedra (i.e., tetrahedra or 7-/8- coordinate polyhedra) are known [9], and also that mixed fluorides with ligands other than F^- do exist, for example vanadium oxide-fluorides [14,15] or fluorides incorporating amines as ligands rather than counterions [16]. Transition metal fluorides are likely to be of interest for a variety of physical properties, for example low-dimensional magnetism [12,14] or as cathode materials for Li or Na-ion batteries [17,18].

Citation: Li, T.; Lightfoot, P. Layered Hybrid iron Fluorides. *Crystals* **2022**, *12*, 1443. https://doi.org/10.3390/cryst12101443

Academic Editor: Višnja Vrdoljak

Received: 20 September 2022
Accepted: 11 October 2022
Published: 13 October 2022

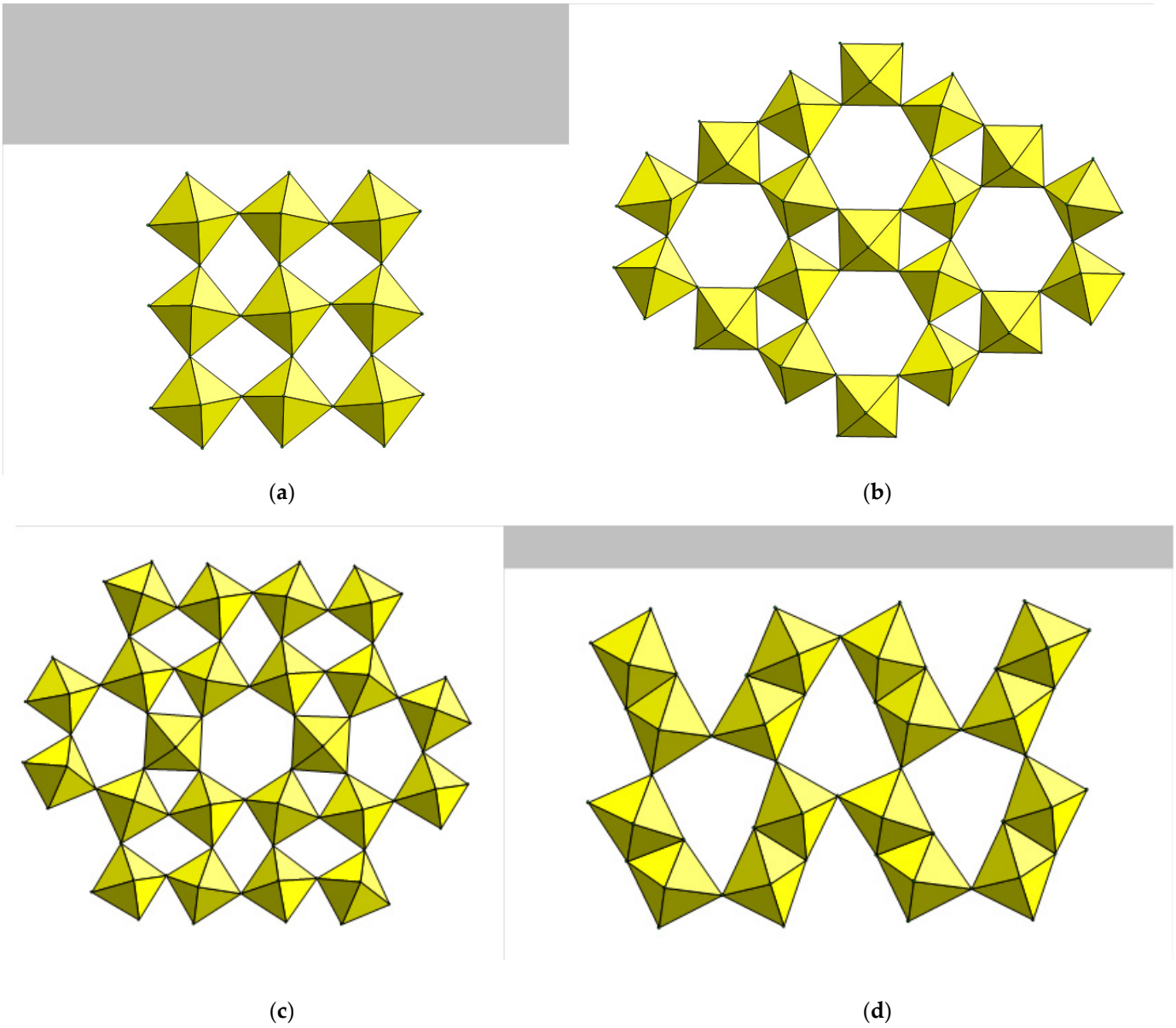

Figure 1. Previously known octahedral layer architectures in hybrid metal fluoride chemistry: (**a**) perovskite-like layer in $[H_2en]MnF_4$ (**b**) kagome layer in $(NH_4)_2[Hea]V_3F_{12}$ (**c**) complex layer in $[H_2en]ScF_4$, containing 3-, 4-, 5- and 6-rings (**d**) edge- and corner-sharing layer in $[H_2pipz]_2Mn_4F_{16}$. Note that all four structures are essentially based on $[MF_4]_\infty$ layers.

Here, we present the first examples of hybrid layered iron fluorides based on the linkage of purely MF_6 octahedra, and using piperazine as a template and structure-directing agent, *viz*. $(H_2pipz)_3Fe_4F_{18}{\cdot}2H_2O$ (**1**) and $(H_2pipz)_2Fe_3F_{13}{\cdot}H_2O$ (**2**). A third related compound, $(H_2pipz)FeF_5{\cdot}H_2O$ (**3**), which exhibits a chain structure, is isolated as the majority product in most of our exploratory reactions in this system. The compounds exhibit new structural features and, since they all crystallise from similar composition regimes, this may suggest that a much wider family of related compounds, using different organic moieties, is still to be discovered.

2. Experimental Section

2.1. Chemicals

Iron (II) fluoride anhydrous (FeF_2, 98%), ferric fluoride anhydrous (FeF_3, $\geq$ 97%), piperazine anhydrous ($C_4H_{10}N_2$, *pipz*, 99%), oxalic acid dihydrate ($C_2H_2O_4{\cdot}2H_2O$, 98%),

hydrofluoric acid (HF, 48–51% wt. in water) and ethylene glycol ($(CH_2OH)_2$, EG, 99%) were purchased from Alfa Aesar. All chemicals were directly used without further purification.

2.2. Synthesis

0.056 g (0.5 mmol) ferric fluoride (FeF_3), 0.172 g (2 mmol) *pipz*, and 0.8 mL (22.4 mmol) HF (48–51% wt. in water) were dissolved in 1 mL EG at room temperature. Then, the homogeneous mixture was sealed in a 15 mL Teflon-lined stainless-steel autoclave and placed in a 120 °C oven, maintained for 120 h. After the autoclave was cooled to room temperature, pure colourless rod single crystals of **3** were obtained by filtration by washing with deionised water.

0.056 g (0.5 mmol) ferric fluoride (FeF_3), 0.086 g (1 mmol) *pipz*, and 0.8 mL (22.4 mmol) HF (48–51% wt. in water) were dissolved in 15 mL EG at room temperature. Then, the homogeneous mixture was sealed in a 30 mL Teflon-lined stainless-steel autoclave and placed in a 120 °C oven, maintained for 120 h. After the autoclave was cooled to room temperature, the product was obtained by filtration by washing with ethanol. There are two crystallised phases in the product, large colourless rod single crystals of compound **3** and small colourless chip single crystals of **1** (approximately 60:40 mixture by mass for the two products). The single crystal products of **1** were picked out manually.

0.094 g (1 mmol) iron fluoride (FeF_2), 0.086 g (1 mmol) *pipz*, and 0.252 g (2 mmol) oxalic acid dihydrate ($C_2H_2O_4{\cdot}2H_2O$) were dissolved in 2 mL EG at room temperature. Then, the homogeneous mixture was sealed in a 50 mL Teflon-lined stainless-steel autoclave and placed in a 120 °C oven, maintained for 96 h. After the autoclave was cooled to room temperature, the product was obtained by filtration with washing by ethanol. There are also two crystallised phases in the product, large rod single crystals of **3** and a small amount of colourless chip single crystals of **2** (approximately 75:25 mixture by mass for the two products). The single crystal products of **2** were picked out manually.

2.3. Characterisation

Single Crystal X-ray diffraction data were collected at 173 K on a Rigaku SCX Mini diffractometer using Mo-K_α radiation (λ = 0.71075 Å). Data were collected using CrystalClear (Rigaku) software [19]. Structures were solved by direct methods using SHELXT [20], and full-matrix least-squares refinements on F^2 were carried out using SHELX-2018/3 [21] incorporated in the WINGX program [22]. Absorption corrections were performed empirically from equivalent reflections on the basis of multi-scans by using CrystalClear [19]. Non-H atoms were refined anisotropically and hydrogen atoms were treated as theoretical riding atoms with the riding code HFIX 23 for carbon-coordinating hydrogen atoms and HFIX 137 for nitrogen-coordinating hydrogen atoms.

Powder X-ray diffraction (PXRD) data of **3** were collected on a PANalytical EMPYREAN diffractometer using Cu $K_{\alpha1}$ (λ = 1.5406 Å) radiation in the range of 3 to 70°, to confirm the purity of the sample. The sample was placed in a rotatable Teflon disc sample holder. Rietveld refinements were carried out using the GSAS package [23] with the EXPGUI interface [24]. The PXRD data of **1** and **2** were not characterized due to the low yield. Unfortunately, further exploratory reactions failed to produce purer samples of **1** and **2**.

Figure 2 shows the Rietveld refinement for the PXRD data of **3**. The refined parameters include background, scale factor, profile parameters (GV, GW, GP and LX), cell parameters, the coordination sites of non-hydrogen atoms and U_{iso} for Fe. The crystallographic model was used, based on the CIF file from the single crystal refinement at 173 K, with a monoclinic space group, $P2_1/n$. The refined lattice parameters are a = 11.5017(5) Å, b = 5.8831(2) Å, c = 13.6393(9) Å and β = 91.306(3)° with wRp = 0.0407, Rp = 0.0282 and χ^2 = 3.657. The result shows no crystallographic phase transition between 173 K and room temperature.

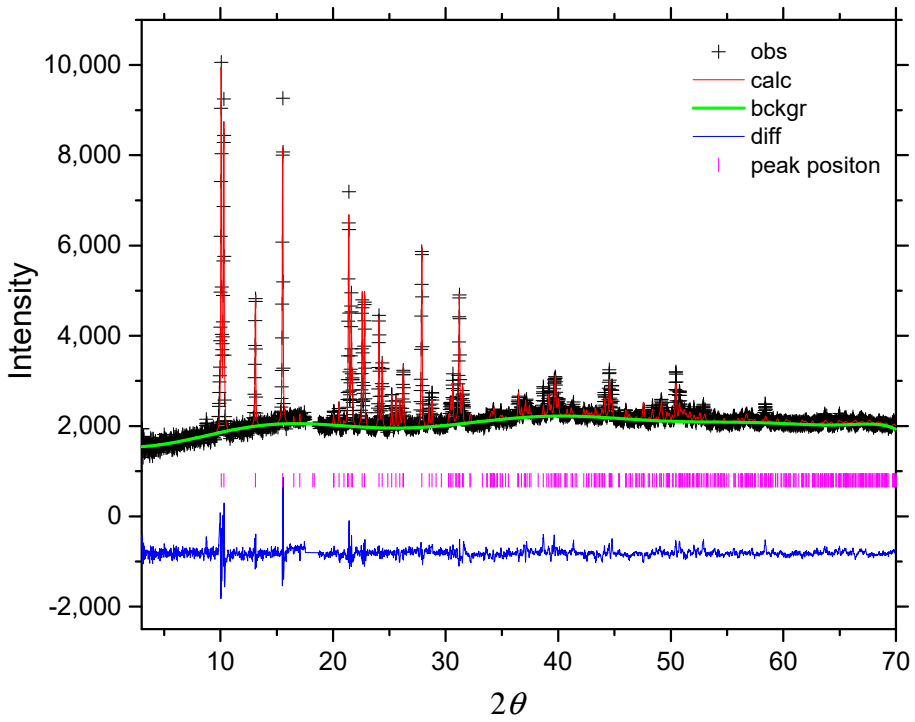

Figure 2. Rietveld plot (PXRD, CuKα1) for **3**. The Teflon peak near 2θ~18° has been excluded from the refinement.

3. Results and Discussion

Crystallographic details (at 173 K) for the three new compounds are given in Table 1. Selected bond lengths are given in Table 2. All three structures incorporate diprotonated piperazine (H_2*pipz*) as a countercation to the anionic iron(III) fluoride layers/chains. In each case, the valence state of the iron is confirmed by bond-valence calculations (Table 2) [25].

Table 1. Crystal and Structure Refinement Data for **1**, **2** and **3** at 173K.

Compound	1	2	3
Formula	$(H_2pipz)_3Fe_4F_{18}\cdot 2H_2O$	$(H_2pipz)_2Fe_3F_{13}\cdot H_2O$	$(H_2pipz)FeF_5\cdot H_2O$
Formula weight	865.90	608.88	257.02
Crystal system	monoclinic	monoclinic	monoclinic
Space group	*P*2/*c*	*C*2/c	$P2_1/n$
a/Å	16.9178(13)	20.5365(14)	11.4695(8)
b/Å	13.6023(10)	13.5405(9)	5.8774(4)
c/Å	12.8848(10)	13.5727(9)	13.6090(10)
β/°	108.530(3)	92.588(4)	91.553(6)
V/Å^3	2811.4(4)	3770.4(4)	917.06(11)
Z	4	8	4
Measured ref	23474	15772	7243
Independent ref	4952 [R(int) = 0.0627]	3321 [R(int) = 0.1532]	1588 [R(int) = 0.0403]
GOOF	1.006	1.014	1.045
Final R indices ($I > 2\sigma(I)$)	R_1 = 0.0331 wR_2 = 0.0843	R_1 = 0.0608 wR_2 = 0.1364	R_1 = 0.0250 wR_2 = 0.0756

Table 2. Selected bond distances (Å) and bond valence sums, S (valence units) for **1**, **2**, and **3**.

Compounds		Bond Lengths	S_{ij}		Bond Lengths	S_{ij}		Bond Lengths	S_{ij}		Bond Lengths	S_{ij}
1	Fe1-F1	1.999(2)	0.389	Fe2-F5	1.945(2)	0.451	Fe3-F6	1.971(2)	0.420	Fe4-F14	2.024(2)	0.364
	Fe1-F1	2.018(2)	0.370	Fe2-F6	1.947(2)	0.448	Fe3-F7	1.9839(8)	0.405	Fe4-F15	2.007(2)	0.381
	Fe1-F2	1.872(2)	0.549	Fe2-F12	1.884(2)	0.531	Fe3-F8	1.914(2)	0.491	Fe4-F16	1.879(2)	0.539
	Fe1-F3	1.876(2)	0.543	Fe2-F13	1.846(2)	0.589	Fe3-F9	1.911(2)	0.494	Fe4-F17	1.9466(5)	0.448
	Fe1-F4	1.910(2)	0.497	Fe2-F14	2.016(2)	0.372	Fe3-F10	1.911(2)	0.494	Fe4-F18	1.874(2)	0.546
	Fe1-F5	1.972(2)	0.419	Fe2-F15	1.970(2)	0.421	Fe3-F11	1.909(2)	0.497	Fe4-F19	1.898(2)	0.512
		∑ Fe1 = 2.767			∑ Fe2 = 2.812			∑ Fe3 = 2.801			∑ Fe4 = 2.790	
2	Fe1-F1	2.008(5)	0.380	Fe2-F1	1.984(5)	0.405	Fe3-F7	1.992(5)	0.396			
	Fe1-F2	1.968(5)	0.423	Fe2-F2	2.027(5)	0.361	Fe3-F8	1.875(5)	0.546			
	Fe1-F3	1.905(5)	0.502	Fe2-F4	1.900(5)	0.509	Fe3-F10	2.020(5)	0.367			
	Fe1-F5	1.883(5)	0.534	Fe2-F6	1.905(5)	0.502	Fe3-F11	1.849(5)	0.584			
	Fe1-F9	1.875(5)	0.544	Fe2-F13	1.939(6)	0.458	Fe3-F12	1.924(6)	0.477			
	Fe1-F12	1.932(6)	0.465	Fe2-F14	1.859(6)	0.568	Fe3-F13	1.932(6)	0.465			
		∑ Fe1 = 2.848			∑ Fe2 = 2.803			∑ Fe3 = 2.835				
3	Fe1-F1	1.9098(11)	0.495	Fe1-F4	1.9833(11)	0.407						
	Fe1-F2	1.9182(11)	0.485	Fe1-F4	1.9967(11)	0.391						
	Fe1-F3	1.9020(11)	0.506	Fe1-F5	1.9052(11)	0.502						
		∑ Fe1 = 2.786										

The building unit of **1** consists of a Y-shaped tetramer of octahedrally coordinated Fe centres (Figure 3) where the Fe(2) polyhedron shares a common edge with the Fe(4) polyhedron, and common corners with Fe(1) and Fe(3). This unit has been previously seen in a family of vanadium oxyfluorides, where it has been shown that the tetramers may exist as either isolated units, or linked into chains or layers [15,26]. Indeed, **1** is essentially isostructural to $(H_2pipz)_3V^{III}{}_3V^{IV}F_{17}O{\cdot}1.5H_2O$, but it represents a pure fluoride analogue of this oxyfluoride. The Y-shaped tetrameric groups are connected through the further alternate corner- and edge-sharing pathways to form a 2D flat layer composed of $[Fe_{18}]$ rings (Figure 4a). The 2D layers are stacked in a staggered style along the *b*-axis (Figure 4b). The H_2pipz^{2+} cations locate in the interlayer positions and link the neighbouring $[Fe_{18}]$ rings through hydrogen bonds thus forming the 3D structure (Figure 4c).The channel H_2O molecules are located in the cavity of the $[Fe_{18}]$ rings and connect the layer structure through O1s-H—F18, O1s'-H—F18, O1s'-H—F3 and O2s-H—F19 with the O—F distances 2.418(7), 2.485(10), 2.856(13) and 2.846(7) Å, respectively.

Compound **2** also adopts a complex layer structure, which may be regarded as built up from trimeric (V-shaped) units of linked FeF_6 octahedra (Figure 5). These trimeric units are connected through edge-sharing pathways to form a 2D flat layer with $[Fe_{14}]$ rings (Figure 6a), within which the H_2O molecules sit and interact with the inorganic layers through hydrogen bonds, with O1s-H—F9 and O1s-H—F14 with distances of 2.895(17) and 2.770(17) Å. The 2D layers are stacked in a staggered style along the *c*-axis (Figure 6b) and the inter-layer piperazinium moieties again act to form hydrogen bonds to the inorganic layers (Figure 6c). As far as we are aware this type of $[Fe_{14}]$ ring is unique within metal fluoride crystallography. Compound **3** features a *cis*-corner-sharing infinite chain moiety $[FeF_5]_\infty$ which has been observed in several transition metal fluorides systems [27] including the vanadium analogue $(H_2pipz)VF_5{\cdot}H_2O$ [26].

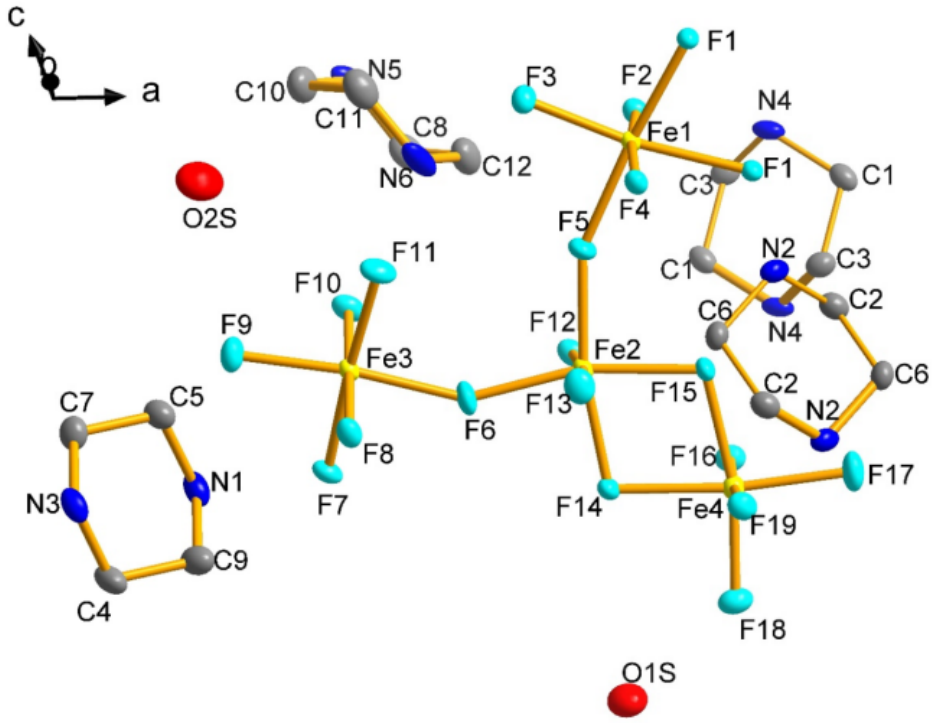

Figure 3. The building unit of **1** (Hydrogen atoms are eliminated for clarity).

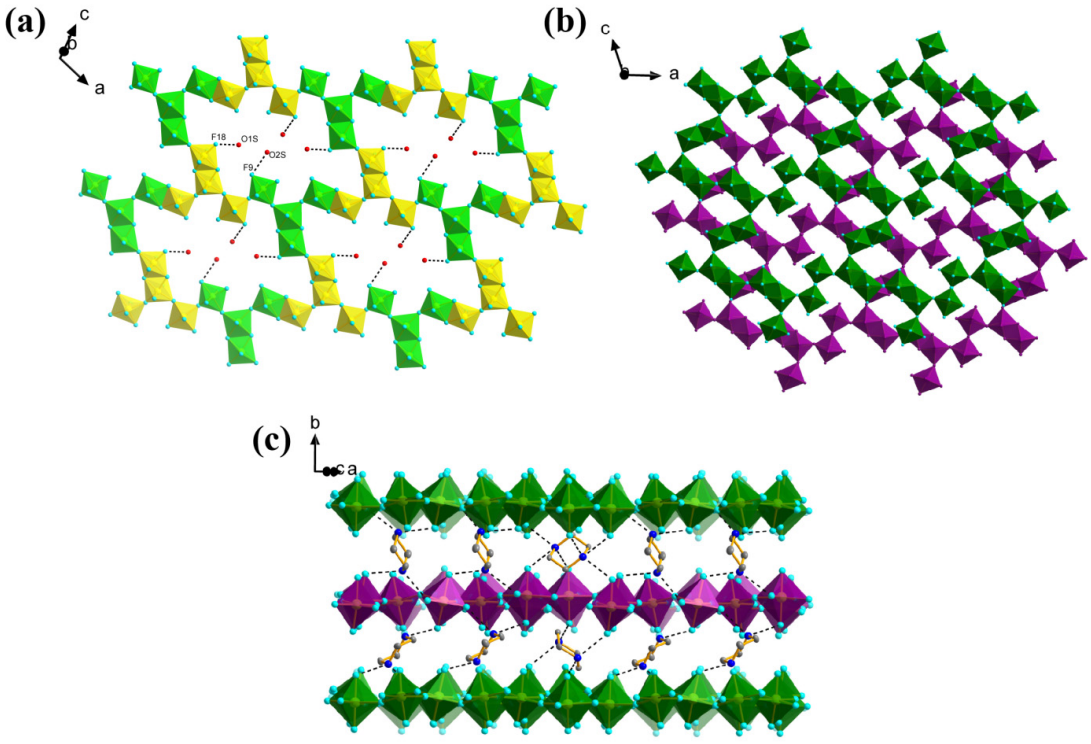

Figure 4. (**a**) The 2D layers with channel water molecules of **1**. The octahedra with different colours show how the "Y" shaped Fe-F building units are connected. (Hydrogen bonds are depicted by dotted lines); (**b**) Plan view of the layer stacking, with different layers shown in different colours. (H_2*pipz* and water molecules are eliminated for clarity); (**c**) The stacking of the layers with H_2*pipz* along the *b*-axis (Selected hydrogen atoms are eliminated for clarity but hydrogen bonds are depicted by dotted lines).

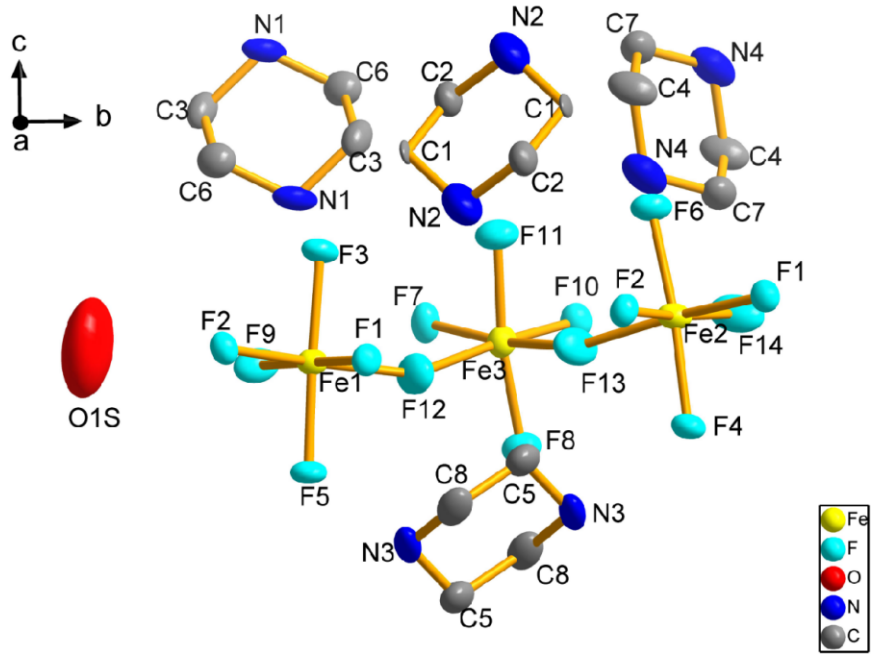

Figure 5. The building unit of **2** (Hydrogen atoms are eliminated for clarity).

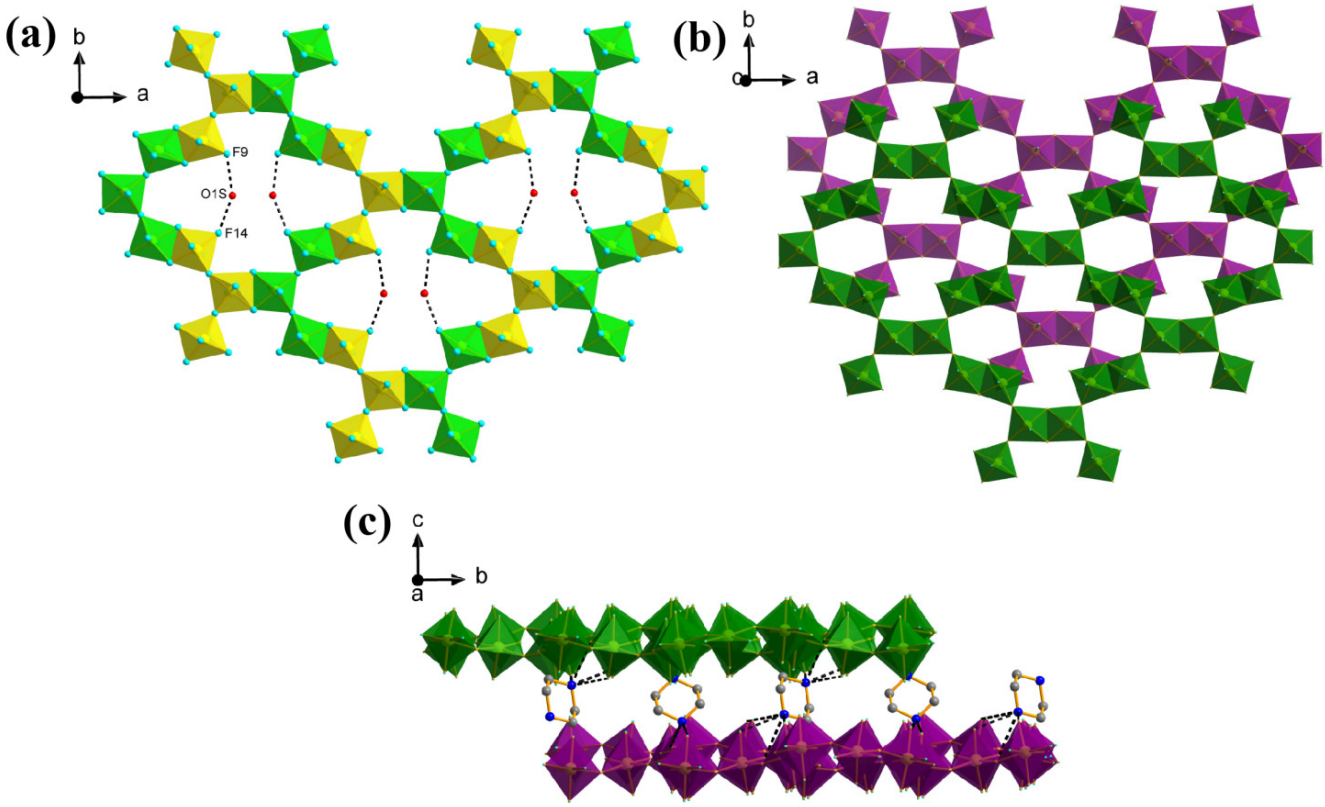

Figure 6. (**a**) The 2D layers with channel water molecules of **2**. The octahedra with different colours show how the "V" shaped Fe-F building units are connected. (Hydrogen bonds are depicted by dotted lines); (**b**) Plan view of the layer stacking with different layers are shown in different colours. (H_2*pipz* and water molecules are eliminated for clarity); (**c**) The stacking of the layers with H_2*pipz* along the *c*-axis of **2** (Selected hydrogen atoms are eliminated for clarity but hydrogen bonds are depicted by dotted lines.).

4. Conclusions

In conclusion, we have prepared three new hybrid iron fluorides, most importantly the first two examples of two-dimensional (i.e., layered) crystal structure within this family, both of which display F/*M* ratios different to those of the known $[MF_4]_\infty$ type layers shown in Figure 1. These initial explorations have focused on using piperazinium as a structure-directing/templating agent. Obviously there will be a huge variety of opportunities for related chemistry using different organic moieties. In the reactions carried out so far, compound **3**, $(H_2pipz)FeF_5{\cdot}H_2O$, always occurs as the main phase, with compounds **1**, $(H_2pipz)_3Fe_4F_{18}{\cdot}2H_2O$, and **2**, $(H_2pipz)_2Fe_3F_{13}{\cdot}H_2O$, being isolated from some reactions as major impurities. Compounds **1** and **2** may be regarded, compositionally and structurally, as a kind of homologous series: both are based open $[Fe_x]$-ring layer structures in which the layers are stacked in a similar, 'staggered' style. The compounds also correspond to a homologous composition series $(H_2pipz)_nFe_{(n+1)}F_{(5n+3)}{\cdot}x(H_2O)$ (n = 1, 2, 3, ...) with n = 3 in the case of **2** and n = 2 for compound **3**. The unit "$(pipzH_2)FeF_5{\cdot}x(H_2O)$" may then be regarded as the differential moiety, relating one homologue to the next. Thus, for example, when n = 1, the formula would $(H_2pipz)Fe_2F_8{\cdot}x(H_2O)$, or more simply, based on a $[FeF_4]_\infty$ layer. There are various possibilities for the connectivity of an iron fluoride layer of this stoichiometry (see Figure 1). One possibility, for example, can be considered as a perovskite-like layer, forming a $[Fe_4]$ ring structure with the octahedral connection in corner-shared style only. Other possibilities are kagome, or tungsten-bronze types. Such structures are common in inorganic-only fluoride chemistry. Except for these types based on purely corner-sharing, there are also many other $[FeF_4]_\infty$ layers which could form by edge-sharing or mixed sharing of octahedra. Further exploratory work in related systems is expected to produce many interesting new structure types, with potentially interesting electronic or magnetic properties.

Supplementary Materials: The following supporting information can be downloaded at: https://www.mdpi.com/article/10.3390/cryst12101443/s1.

Author Contributions: T.L. carried out all the chemistry, crystallography and further characterisation. P.L. coordinated the project and writing of the paper, with the approval of T.L. All authors have read and agreed to the published version of the manuscript.

Funding: This research was funded by the China Scholarship Council and the University of St Andrews joint fundation (201606280032, PhD studentship to T.L.) and the China Postdoctoral Science Foundation (2022M710619). The APC was funded by author voucher discount.

Data Availability Statement: Further details of the crystal structures can be obtained from the CCDC (https://www.ccdc.cam.ac.uk, accessed on 28 September 2022) on quoting deposition numbers 2206993-2206995 for compounds **1**–**3**.

Acknowledgments: We thank D. Cordes for helpful discussions.

Conflicts of Interest: The authors declare no conflict of interest.

References

1. McNulty, J.A.; Lightfoot, P. Structural chemistry of layered lead halide perovskites containing single octahedral layers. *IUCrJ* **2021**, *8*, 485–513. [CrossRef] [PubMed]
2. Li, X.T.; Hoffman, J.M.; Kanatzidis, M.G. The 2D halide perovskite rulebook: How the spacer influences everything from the structure to optoelectronic device efficiency. *Chem. Rev.* **2021**, *121*, 2230–2291. [CrossRef] [PubMed]
3. Mercier, N.; Louvain, N.; Bi, W. Structural diversity and retro-crystal engineering analysis of iodometalate hybrids. *CrystEngComm* **2009**, *11*, 720–734. [CrossRef]
4. Han, J.; Nishihara, S.; Inoue, K.; Kurmoo, M. On the nature of the structural and magnetic phase transitions in the layered perovskite-like $(CH_3NH_3)_2[FeIICl_4]$. *Inorg. Chem.* **2014**, *53*, 2068–2075. [CrossRef]
5. Worley, C.; Yangui, A.; Roccanova, R.; Du, M.-H.; Saparov, B. $(CH_3NH_3)AuX_4{\cdot}H_2O$ (X = Cl, Br) and $(CH_3NH_3)AuCl_4$: Low-band gap lead-free layered gold halide perovskite materials. *Chem. Eur. J.* **2019**, *25*, 9875–9884. [CrossRef] [PubMed]
6. Vishnoi, P.; Zuo, J.L.; Li, X.T.; Binwal, D.C.; Wyckoff, K.E.; Mao, L.; Kautzsch, L.; Wu, G.; Wilson, S.D.; Kanatzidis, M.G.; et al. Hybrid layered double perovskite halides of transition metals. *J. Am. Chem. Soc.* **2022**, *144*, 6661–6666. [CrossRef]

7. Han, C.; McNulty, J.A.; Bradford, A.J.; Slawin, A.M.Z.; Morrison, F.D.; Lee, S.L.; Lightfoot, P. Polar ferromagnet induced by fluorine positioning in isomeric layered copper halide perovskites. *Inorg. Chem.* **2022**, *61*, 3230–3239. [CrossRef]
8. Ben Ali, A.; Greneche, J.M.; Leblanc, M.; Maisonneuve, V. $[H_3tren]^{3+}$ templated iron fluorides; synthesis, crystal structures and Mössbauer studies. *Solid State Sci.* **2009**, *9*, 1631–1638. [CrossRef]
9. Adil, K.; Leblanc, M.; Maisonneuve, V.; Lightfoot, P. Structural chemistry of organically-templated metal fluorides. *Dalton Trans.* **2010**, *39*, 5983–5993. [CrossRef]
10. Stephens, N.F.; Slawin, A.M.Z.; Lightfoot, P. A novel scandium fluoride, $[C_2N_2H_{10}]_{0.5}[ScF_4]$, with an unprecedented tungsten bronze-related layer structure. *Chem. Commun.* **2004**, 614–615. [CrossRef]
11. Stief, R.; Massa, W.Z. Jahn-Teller ordering in $pipzH_2[Mn_2F_8]$, a fluoromanganate(III) with a new layer structure. *Anorg. Allg. Chem.* **2006**, *632*, 797–800. [CrossRef]
12. Aidoudi, F.H.; Downie, L.J.; Morris, R.E.; de Vries, M.A.; Lightfoot, P. A hybrid vanadium fluoride with structurally isolated S = 1 kagome layers. *Dalton Trans.* **2014**, *43*, 6304–6307. [CrossRef] [PubMed]
13. Li, T.; Clulow, R.; Bradford, A.J.; Lee, S.L.; Slawin, A.M.Z.; Lightfoot, P. A hybrid fluoride layered perovskite, $(enH_2)MnF_4$. *Dalton Trans.* **2019**, *48*, 4784–4787. [CrossRef] [PubMed]
14. Aidoudi, F.H.; Aldous, D.W.; Goff, R.J.; Slawin, A.M.Z.; Attfield, J.P.; Morris, R.E.; Lightfoot, P. An ionothermally-prepared S = 1/2 kagome lattice. *Nat. Chemistry.* **2011**, *3*, 801–806. [CrossRef] [PubMed]
15. DeBurgomaster, P.; Ouellette, W.; Liu, H.; O'Connor, C.J.; Yee, G.T.; Zubieta, J. Solvatothermal chemistry of organically-templated vanadium fluorides and oxyfuorides. *Inorg. Chim. Acta.* **2010**, *363*, 1102–1113. [CrossRef]
16. Pimenta, V.; Le, Q.H.H.; Clark, L.; Lhoste, J.; Hémon-Ribaud, A.; Leblanc, M.; Grenèche, J.M.; Dujardin, G.; Lightfoot, P.; Maisonneuve, V. New iron tetrazolate frameworks: Synthesis temperature effect, thermal behaviour, Mössbauer and magnetic studies. *Dalton Trans.* **2015**, *44*, 7951–7955. [CrossRef]
17. Song, H.; Yang, G.; Cui, H.; Wang, C. Honeycomb-like porous iron fluoride hybrid nanostructure: Excellent Li-storage properties and investigation of the multi-electron reversible conversion reaction mechanism. *J. Mater. Chem. A* **2015**, *3*, 19832–19841. [CrossRef]
18. Lemoine, K.; Zhang, L.T.; Greneche, J.M.; Hemon-Ribaud, M.; Leblanc, M.; Guiet, A.; Galven, C.; Tarascon, J.M.; Maisonneuve, V.; Lhoste, J. New amorphous iron-based oxyfluorides as cathode materials for high-capacity lithium-ion batteries. *J. Phys. Chem. C* **2019**, *123*, 21386–21394. [CrossRef]
19. Rigaku. *CrystalClear 2014*; Rigaku Corporation: Tokyo, Japan, 2014.
20. Sheldrick, G.M. Crystal structure refinement with SHELXL. *Acta Cryst. Sect. C Struct. Chem.* **2015**, *71*, 3–8. [CrossRef]
21. Sheldrick, G.M. *SHELXL-2018*; Program for the Refinement of Crystal Structures; University of Göttingen: Göttingen, Germany, 2018.
22. Farrugia, L.J. WinGX and ORTEP for Windows: An update. *J. Appl. Cryst.* **2012**, *45*, 849–854. [CrossRef]
23. Larson, A.C.; Von Dreele, R.B. *General Structure Analysis System (GSAS)*; Los Alamos National Laboratory: Los Alamos, NM, USA, 2004.
24. Toby, B.H. EXPGUI, a graphical user interface for GSAS. *J. Appl. Cryst.* **2001**, *34*, 210–213. [CrossRef]
25. Brese, N.E.; O'Keeffe, M. Bond-valence parameters for solids. *Acta Cryst. B* **1991**, *47*, 192–197. [CrossRef]
26. Aldous, D.W.; Stephens, N.F.; Lightfoot, P. The role of temperature in the solvothermal synthesis of hybrid vanadium oxyfluorides. *Dalton Trans.* **2007**, 4207–4213. [CrossRef]
27. Leblanc, M.; Maisonneuve, V.; Tressaud, A. Crystal chemistry and selected physical properties of inorganic fluorides and oxide-fluorides. *Chem. Rev.* **2015**, *115*, 1191–1254. [CrossRef] [PubMed]